Chemical Engineering Science 73 (2012) 334–344

Contents lists available at SciVerse ScienceDirect

Chemical Engineering Science

journal homepage: www.elsevier.com/locate/ces

Experimental study of water wetting in oil–water two phase flow—Horizontal flow of model oil

Jiyong Cai [1], Chong Li [1], Xuanping Tang, Francois Ayello [2], Sonja Richter *, Srdjan Nesic

Institute for Corrosion and Multiphase Technology, Ohio University, 342 West State Street, Athens, OH 45701, USA

ARTICLE INFO

Article history:
Received 8 July 2011
Received in revised form
10 December 2011
Accepted 10 January 2012
Available online 1 February 2012

Keywords:
Water wetting
Multiphase flow
Oil–water flow
Wettability
Horizontal flow
Corrosion

ABSTRACT

When crude oil and water are simultaneously transported in mild steel pipelines, corrosion problems are generally associated with the water phase being in contact with the metal surface at the bottom of the pipe. Consequently, knowing whether oil or water wets the pipe wall is an important factor, which can affect the corrosion mitigation strategy and increase confidence in the integrity of the pipeline. There are large knowledge gaps in this area of research and consequently only very crude empirical criteria are used in the industry.

In the present work an experimental study of oil–water flow was conducted in a large diameter (0.1 m ID) horizontal multiphase flow loop using four measurement techniques: flow pattern visualization, conductivity pins, fluid sampling and monitoring of corrosion rate via ferrous ion concentration (iron count). Five different oil/water flow patterns were observed and a flow regime map was constructed. The flow patterns were smooth stratified flow, stratified flow with water globules, stratified flow with mixing layer, semi-dispersed flow and dispersed flow. The results from the conductivity pins showed three different wetting behaviors: stable water wetting, stable oil wetting and intermittent wetting. The results of the fluid sampling were consistent with the wetting results from the conductivity pins. Ferrous ion monitoring demonstrated that corrosion occurs only when water wets the pipe walls and is greater for stable water wetting than for intermittent wetting.

1. Introduction

Corrosion in oil and gas pipelines can be attributed to the presence of dissolved gases, such as CO_2 and/or H_2S, in water. The hydrocarbon phase is by itself not considered corrosive and can even be inhibitive (Efird and Jasinski, 1989; Hernandez et al., 2002; Hernandez et al., 2003; Mendez et al., 2001). In theory, a pipeline would be free of corrosion problems if the water phase was entirely entrained by the oil phase, rather than flowing freely at the bottom. Therefore, for given flow rates in a line and certain fluids properties, it would be important to know when the conditions of oil vs. water wetting will occur. This knowledge can help increase the confidence in the measures taken to ensure integrity of the pipeline and decreases costs and the environmental impact.

In oil–water flow through a horizontal line, at lower flow rates, the gravitational force dominates over the turbulent force and the water phase flows as a separate layer in a stratified flow regime. As the flow rate increases, the turbulence energy of the flow increases and the water becomes gradually more dispersed in the oil phase. This process may appear different at very high water cuts, above the so called "phase inversion point" (Brauner and Ullmann, 2002), where the oil is dispersed in the continuous water phase and the pipe wall is predominantly wetted by water. In the present work, the focus is on low water cuts (less than 20%) where oil is the continuous phase, which is a more realistic situation in the field.

1.1. Flow pattern determination and analysis

For gas–liquid two-phase flow, the flow patterns can be divided into either *stratified*, *intermittent* (elongated bubble, slug, wavy annular), *annular* or *dispersed bubble* flow. In oil–water flow, the distinction between flow patterns is not as clear as for gas–liquid flow due to the smaller difference in fluids densities. Consequently the researchers do not always report the same flow patterns, although sometimes a very similar flow pattern is reported with different names. Flow pattern designations for oil–water flow proposed by Trallero (1995) are widely used as a benchmark by other researchers (Kumara et al., 2009; Rodriguez and Oliemans, 2006; Simmons and Azzopardi, 2001; Utvik et al., 2001; Xu, 2007). The key flow patterns can be divided into two

* Corresponding author. Tel.: +1 740 593 9947; fax: +1 740 593 9949.
E-mail address: richtes1@ohio.edu (S. Richter).
[1] Present address: ExxonMobil, ExxonMobil Upstream Research Company, Gas & Facilities Division, P.O. Box 2189, Houston, TX 77252, USA.
[2] Present address: DNV Columbus, 5777 Frantz Road, Dublin, OH 43017, USA.

0009-2509/$ - see front matter © 2012 Elsevier Ltd. All rights reserved.
doi:10.1016/j.ces.2012.01.014

main groups, *stratified* and *dispersed*. The stratified flow patterns are further divided into *stratified flow* and *stratified flow with mixing layer* (water layer at bottom, oil layer on top with a dispersion of oil and water in the middle), and the dispersed flow patterns are divided into *dispersion of oil in water and water* (free water layer at bottom and dispersed layer on top), *dispersion of oil in water and water in oil* (two layer dispersion), *water in oil emulsion* and *oil in water emulsion*.

In addition to the flow patterns identified by Trallero (1995), Nädler and Mewes (1997) identified a three layer flow structure consisting of a *water-in-oil dispersion* on top of a *oil-in-water dispersion and water layer*. Angeli and Hewitt (2000) reported a *stratified wavy* flow pattern, which might have been observed by other researchers as *stratified* (Nadler and Mewes, 1997; Rodriguez and Oliemans, 2006; Trallero, 1995; Utvik et al., 2001). None of the researchers mentioned above reported the *annular flow* pattern, which tends to occur when the viscosity of the oil is high, with a critical value of 0.035 Pa s suggested by Xu (2007), and if the density of the oil is close to the density of water (Bannwart et al., 2004; Charles et al., 1961) or if the pipe diameter is very small (Mandal et al., 2007; Wegmann and von Rohr, 2006). Oil–water flow patterns are not as sensitive to the pipe diameter as gas–liquid flow patterns, which need large-diameter (larger than 0.075 m) in order to adequately represent in-situ large diameter pipeline flow (Jepson and Taylor, 1993). Oil–water flow patterns seem to depend more on the properties of the liquids, such as interfacial tension, density and viscosity, and somewhat less on pipe diameter, although different flow patterns were observed for very small diameter pipes (10 mm and smaller), where flow patterns such as *plug*, *slug*, *churn* and *rivulet* occur (Mandal et al., 2007).

The transition from separated flow to dispersed flow is usually not explicitly reported in oil–water two phase flow research, but the value can be deducted from the published flow patterns. In the case of Angeli and Hewitt (2000), this transition was found at V_{so}=1.5 m/s, for an acrylic 0.025 m pipe and oil with viscosity of 0.0016 Pa s and interfacial tension of 0.017 N/m. In the work of Trallero et al. (1996) this transition was measured at V_{so}=0.8 m/s for a larger pipe (0.05 m diameter) and a model oil with higher viscosity (0.029 Pa s) and higher interfacial tension (0.036 N/m). However, Simmons and Azzopardi (2001) found the transition at 2.4 m/s for even larger pipe (0.063 m diameter) and oil viscosity of 0.0018 Pa s. The exact transition velocity between stratified and dispersed flow is obiously dependent on the pipe diameter, and the oil properties. The general trend is for the transition to move to higher oil velocities for larger diameter pipes but to lower oil velocities for higher oil viscosity, higher oil density and lower interfacial tensions.

1.2. Water entrainment modeling

When modeling CO_2 corrosion in oil pipelines, it is of utmost importance to account for the distribution of the entrained water phase—whether it is dispersed in the oil phase (leading to oil wetting of the line internal wall) or flowing separated at the bottom of the pipe (leading to water wetting and corrosion of the mild steel pipe internal surface). Making the wrong prediction of the type of wetting would lead to erroneous prediction of the corrosion rate and possibly much higher capital costs (due to use of more corrosion resistant materials) and/or higher operational costs (due to overuse of corrosion inhibitor).

The prediction of wetting in the industry has been incorporated into some CO_2 corrosion prediction models typically as a "rule-of-thumb". In the case of a model proposed by Simon Thomas et al. (1987), oil wetting was expected to occur in pipelines when the water cut was less than 20% and the flow velocity higher than 1 m/s. Later, these values were revised to a critical flow velocity of 1.5 m/s and water cuts up to 40% (Pots et al., 2002). Adams et al. (1993) were less conservative in their wetting prediction and concluded that oil wetting would occur for water cuts less than 30%, independent of flow velocity. de Waard and Lotz (1993) also predicted that oil wetting would occur for water cuts less than 30%, but only if the oil velocity was greater than 1 m/s. Later, de Waard et al. (2001) extended the influence of the oil phase with an empirical multiplier which took into an account the crude oil type, the water cut and inclination but did not take the pipe diameter into account. Despite the slight improvement of the empirical models over the simple "rule-of-thumb" approach, both approaches remain questionable and do not provide any insight into the mechanism of water entrainment and separation. Moreover, they are only valid for the conditions (fluid properties, pipe diameter, inclination, etc.) for which they were constructed and therefore lack generality. Any extrapolation is uncertain and therefore unreliable.

Another approach to assess the effect of phase wetting on CO_2 corrosion is to create a mechanistic model based on simplified physics underpinning oil–water pipe flow. We can start with the classical work of Hinze (1955), who investigated the forces involved when droplets are dispersed in a continuous phase. The balance of forces can be best decribed with the dimensionless Weber number, *We*, which is a ratio between the external force (τ) which wants to break the droplet up and the opposing surface tension force (σ/d_{max}), where σ is the interfacial tension (N/m) and d_{max} (m) is the size of the largest droplet which the turbulent flow can sustain.

$$We = \frac{\tau d_{max}}{\sigma} \tag{1}$$

The fundamental work of Hinze (1955) was used as a base for an entrainment model published by Wicks and Fraser (1975). The model predicts an increase in the entrainment velocity with increasing internal diameter of the pipeline and increasing interfacial tension, which is correct, but it does not take the water cut into account. Moreover, the model uses the Weber number for droplets being broken up in an air stream, rather than emulsification in liquid and is calibrated against data for sand entrainment. The resulting entrainment velocity is low and in practice only valid for very low water cuts.

Wu (1995) modified the Wicks and Fraser (1975) model to include the critical Weber number for emulsification in turbulent flow (Hinze, 1955) where, instead of using the maximum velocity of the stream, only the velocity fluctuation ($\bar{v}$) that occurs over distances close to the size of the droplets are effective in breaking them up. That is to say, smaller eddies are more efficient in the break-up of the droplet than larger eddies, which presumably only sweep the droplets along, just like the main flow does. This is described by Eq. (2), with ρ_o being the density (kg/m^3) of the continuous phase, i.e. the oil phase in this case.

$$We_{crit} = \frac{\rho_o \bar{v}^2 d_{max}}{\sigma} \tag{2}$$

Wu (1995) furthermore proposed a critical droplet size, derived from the work of Brauner and Moalem Maron (1992) for horizontal flow. By introducing more realistic force balance and taking into an account the effect of the water phase, Wu significantly improved the original Wicks and Fraser (1975) model.

The Hinze (1955) model was based on single droplets, and does not take coalescence into account. This is valid for dilute dispersions when the criterion in Eq. (3) is valid, where the subscripts *c*, *d* and *m* refer to the continuous phase, the dispersed

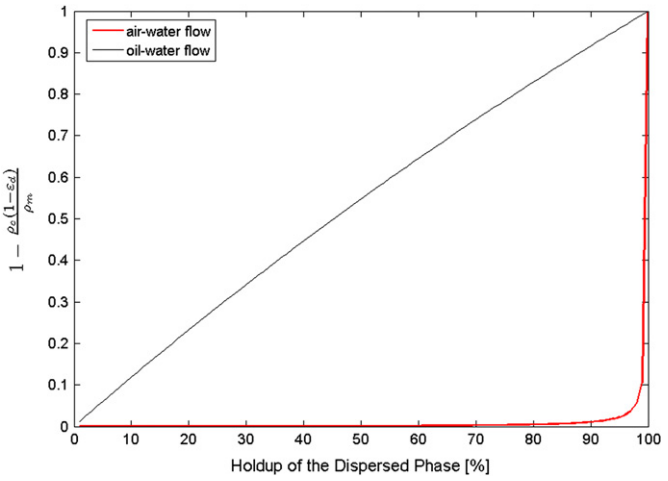

Fig. 1. Criterion for dilute dispersions for air–water and oil–water two phase flows. The criterion is valid when $1-\rho_c(1-\varepsilon_d)/\rho_m \cong 0$, and is drawn up for $\rho_{air}=1.2$ kg/m^3, $\rho_{water}=1000$ kg/m^3 and $\rho_{oil}=825$ kg/m^3.

phase and the mixture, respectively, and ε refers to the hold-up.

$$\rho_c(1-\varepsilon_d)/\rho_m \cong 1 \tag{3}$$

The mixture density is calculated as the weighted average of the two phases based on the hold-up of the dispersed phase:

$$\rho_m = (1-\varepsilon_d)\rho_c + \varepsilon_d\rho_d \tag{4}$$

In Fig. 1 the criterion from Eq. (3) is valid for values close to zero. This will apply for gas–liquid flow for a hold-up of the gas phase up to 80–90% (Fig. 1), whereas for oil–water flow, this criterion is only valid for very low water cuts ($\leq 1\%$) due to the relatively small density difference between oil and water. Therefore, it is more correct that an oil–water dispersion is considered as a dense dispersion, and coalescence between droplets cannot be ignored.

Brauner (2001) was the first to expand on the Hinze (1955) model to incorporate droplet coalescence occurring in dense dispersions. This was achieved by assuming that the oil phase needs to supply sufficient energy to both disperse the water phase and prevent the coalescence of water droplets. Brauner's (2001) is adapted here for the case of water-in-oil dispersions. Eq. (5) expresses the rate of turbulent energy supplied by the oil phase which is balanced with the rate of surface energy creation by the formation of water droplets, where C_H is a constant equal to 1, and Q_o and Q_w are the flow rates of oil and water, respectively. Eq. (6) expresses the squared mean velocity fluctuation, $\overline{v}$ in turbulent flow in terms of the rate of turbulent dissipation, $\overline{e}$ (Hinze, 1955), while Eq. (7) expresses the mean rate of energy dissipation in pipe flow expressed in the terms of the friction factor, f. The friction factor used is the Fanning friction factor, which for turbulent flow can be approximated as $f=0.046(Re)^{-0.2}$ (Knudsen and Katz, 1954), and is valid for Reynolds numbers ranging from 3000 to 3,000,000 where $Re=\rho_o D U_o/\mu_o$ and μ_o is the dynamic viscosity of the oil phase (Pa s) and D the pipe diameter (m).

$$\frac{\rho_o\overline{v}^2}{2}Q_o = C_H\frac{4\sigma}{d_{max}}Q_w \tag{5}$$

$$\overline{v}^2 = 2(\overline{e}d_{max})^{2/3} \tag{6}$$

$$\overline{e} = 2\frac{\rho_m}{\rho_o(1-\varepsilon_w)}\frac{U_{so}^3 f}{D} \tag{7}$$

here U_{so} refers to the superficial oil velocity (m/s), D and ε_w the water hold-up, e.g., the water cut, calculated based on the flow rates of oil and water: $\varepsilon_w=Q_w/(Q_w+Q_o)$, and takes a value from 0 (no water) to 1 (full pipe water flow). By applying Eq. (7) to Eq. (6) the following expression of the maximum droplet size, d_{max}, is derived from Eq. (5):

$$d_{max} = 2.22D\left(\frac{\rho_o U_{so}^2 D}{\sigma}\right)^{-0.6}\left(\frac{\rho_m}{\rho_o(1-\varepsilon_w)}f\right)^{-0.4}\left(\frac{\varepsilon_w}{1-\varepsilon_w}\right)^{0.6} \tag{8}$$

Eq. (8) can be used to calculate the maximum droplet diameter that can be sustained in a turbulent flow, depending on the velocity of the continuous phase (the oil velocity in the case of water-in-oil dispersion), pipe diameter, water cut and the fluid properties, such as interfacial tension between oil and water, density of the oil and the water phase and the oil dynamic viscosity. It should be noted that the water cut, ε_w, describes the inlet conditions of the flow rate for oil and water, and not the local water fraction along the length of the pipe.

While Eq. (8) predicts the size of the maximum droplet in the flow, it does not predict whether this droplet will be suspended by turbulence or "sink" towards the wall due to gravity for example, i.e., whether the flow pattern will be dispersed or stratified. The transition between dispersed and stratified flow is achieved by comparing the *maximum* droplet size to a *critical* droplet size, d_{crit} (m). There are two scenarios possible for a droplet to "fall out" of the flow and move towards the pipe wall. One is due to gravity, which tends to pull the droplet down and the other due to deformation of the droplet, which tends to destabilize the shape of the droplet in the flow and cause it to "swerve" towards the pipe walls. The gravity factor tends to dominate at horizontal and near-horizontal inclinations while the deformation factor is more important in vertical and near-vertical inclinations where gravity plays a negligible role (Barnea, 1986). In order to determine which mechanism and consequently which droplet size is more important, the smaller "critical" droplet diameter is chosen from the two according to Barnea (1986):

$$d_{crit} = min\left(d_{crit}^{gravity}, d_{crit}^{deformation}\right) \tag{9}$$

When the maximum droplet size sustainable in turbulent flow is smaller than the critical droplet size, $d_{max} < d_{crit}$, this suggests that all the droplets in the flow are small enough to be suspended by turbulence and the flow is dispersed. On the other hand, when the maximum droplet size is larger than the critical droplet size, $d_{max} > d_{crit}$, large enough droplets will form in the flow which tend to separate out and flow stratified along the pipeline walls.

The critical droplet size due to gravity is calculated using a force balance between the radial component of the gravitational force, F_G, pushing the droplet towards the wall (Eq. (10)) and the turbulent force, F_T, keeping the droplet suspended (Eq. (11)).

$$F_G = |\Delta\rho| g\cos\beta\frac{\pi d^3}{6} \tag{10}$$

$$F_T = \frac{1}{2}\rho_o u'^2\frac{\pi d^2}{4} \tag{11}$$

where g is the gravitational constant (m^3/kg s), d is the droplet diameter (m), $\Delta\rho$ is the difference in the density between the oil and the water and β is the inclination of the pipe with horizontal as 0° and vertical as 90°. The parameter u' describes the radial velocity fluctuation which is estimated to be equal to the friction velocity $U_f=U_o(f/2)^2$ (Barnea, 1986). The critical droplet size due to gravity, $d_{crit}^{gravity}$, is obtained when $F_G=F_T$ and is expressed by the following equation:

$$d_{crit}^{gravity} = \frac{3}{8}\frac{\rho_o f U_o^2}{|\Delta\rho| Dg\cos\beta} \tag{12}$$

The critical droplet size due to deformation can be calculated as in Eq. (13), based on Stokes theory of terminal velocity for a

solid sphere (Barnea et al., 1982; Bond and Newton, 1928; Brodkey, 1995). When the droplet is smaller than $d_{crit}^{deformation}$, it behaves like a rigid sphere, but if the droplet is larger, it starts to deform and swerve and can fall out of the main flow towards the wall.

$$d_{crit}^{deformation} = \sqrt{\frac{0.4\sigma}{|\Delta\rho| g \cos\beta'}} \tag{13}$$

Brauner (2001) proposed an inclination factor, β', which is positive for downward inclination.

$$\beta' = \begin{cases} |\beta|, & |\beta| \le 45^\circ \\ 90^\circ - |\beta|, & |\beta| > 45^\circ \end{cases} \tag{14}$$

Together, Eqs. (8) and (9) can be used to estimate the transition between dispersed flow (leading to oil wetting) and stratified flow (leading to water wetting) at water cuts below the

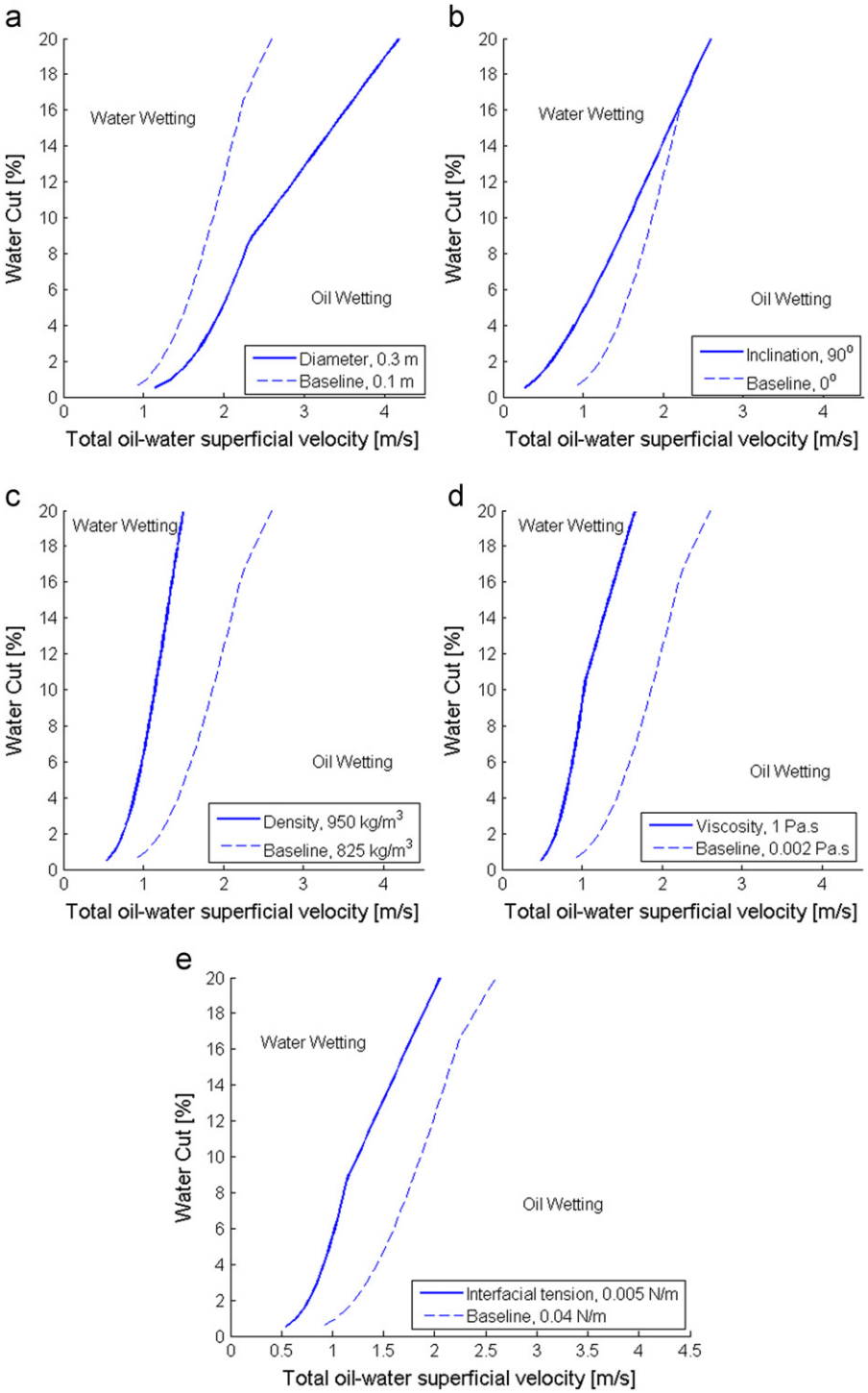

Fig. 2. Predicted transitions between oil and water wetting. All of the graphs have one common set of conditions: "Baseline" (0.1 m horizontal pipe, density 825 kg/m^3, viscosity 0.002 Pa s, interfacial tension 0.04 N/m). The deviation from the baseline is for (a) larger pipe diameter (0.3 m), (b) vertical inclination (90°), (c) higher density (950 kg/m^3), (d) higher viscosity (1 Pa s) and (e) lower interfacial tension (0.005 N/m).

"phase inversion point". Above the "phase inversion point", water becomes the continuous phase and water wetting is predicted to prevail. This model, without being overly complicated, provides much improved oil wetting estimations from earlier "rule-of-thumb" or empirical models.

This approach is a basis of the water wetting model, which is incorporated into the Ohio University mechanistic CO_2 corrosion prediction software package MULTICORP V4.2 (2007). When oil wetting is predicted, the corrosion rate becomes zero, while if water wetting is predicted, the corrosion rate is calculated based on the flow characteristics (such as Reynolds number, water film height, etc.), as well as the water chemistry (Nesic et al., 1996; Nordsveen et al., 2003).

Examples of a transition line obtained by the water wetting model described above are plotted in Fig. 2. On the left side of the transition line, water separation and water wetting are predicted, and on the right side, water dispersion and oil wetting are predicted. On each of the graphs in Fig. 2 the same line is plotted for a common set of conditions—the so called "Baseline". The parameters used in constructing the Baseline are arbitrary and are in this case typical values based on the experimental conditions used in the current research: pipe ID 0.1 m, horizontal (0° inclination) pipe with oil properties of $\rho=825$ kg/m^3, $\mu=0.002$ Pa s and $\sigma=0.04$ N/m. By changing one parameter at a time, while keeping the others constant, some insight can be gained into the general behavior of the model.

The model predicts higher entrainment velocities for larger diameter pipes (Fig. 2(a)). Since the breakup of the droplets is governed by the turbulent velocity fluctuations which occur over the same distance as the size of the droplets, then it follows that larger pipes producing larger eddies are not as efficient in breaking up the droplets as smaller pipes, where the turbulent eddies are smaller.

Inclination (Fig. 2(b)) has the effect of lowering the critical entrainment velocity, making it easier to entrain the water as the inclination is increased, since the gravity component, driving the separation, becomes weaker.

Higher density and viscosity (Fig. 2(c) and (d), respectively) also contribute to lower entrainment velocities, since the water is more easily carried by the oil. However, high interfacial tension works the other way, by making the break-up of the droplet more difficult.

This type of predicted behavior seems to be in accordance with the general field experience when it comes to water wetting, for example heavier, more viscous oils are known to entrain and suspend water more effectively than their lighter counterparts; by adding a corrosion inhibitor or another surface active substance, very low values of interfacial tension can be obtained (around 0.005 N/m or even lower) resulting in smaller, more easily entrained water droplets (Fig. 2(e)). However, a more convincing argument can be made only by comparing the predictions with accurate measurements such as the ones described in the following section.

2. Experimental setup and instrumentation

The experimental program was conducted using a paraffinic LVT200 model oil and water solution with 1 wt% NaCl (prepared with deionized water) both of which are saturated with CO_2 (see Table 1). LVT200 has the viscosity, $\mu=0.002$ Pa s, density, $\rho=825$ kg/m^3 and interfacial tension, $\sigma=0.040$ N/m, at room temperature. In these experiments, the water cut was varied from 1% to 20% and testing was performed at ambient temperature and pressure.

2.1. Experimental layout

The experiments were conducted at the Institute for Corrosion and Multiphase Technology (2007) at Ohio University in a 40 m long, 0.1 m ID multiphase flow loop mounted on a fully inclinable rig. The multiphase flow loop, shown in Fig. 3, is specially designed to investigate internal corrosion and multiphase pipe flow under realistic flow conditions found in the field. The results in the current paper are focused on horizontal conditions (0°).

Table 1
Test parameters for horizontal model oil flow loop testing.

Parameter	Value
Oil phase	LVT200 oil
Water phase	De-ionized water with 1 wt% NaCl
Superficial water velocity, V_{sw}	0–0.22 m/s
Superficial oil velocity, V_{so}	0.5–2.5 m/s
Water cut, ε	0–20%
Pipe inclination	0 deg. (horizontal)
Pipe diameter	4 in.
System temperature	25 °C
System pressure	0.103 MPa

The model oil is stored in a 1.2-m^3 stainless steel storage tank. The tank is equipped with two 1-kW heaters and stainless steel cooling coils to maintain a constant temperature for all tests. Deionized water with 1 wt% NaCl is stored in another 1.2 m^3 stainless steel storage tank. The oil and the aqueous phase are pumped separately using positive displacement pumps equipped with variable speed motors. The oil flow rate is controlled within a range of 0.5–3 m/s superficial velocity with 5% accuracy and the water superficial velocity is controlled within a range of 0.01–1 m/s with 2% accuracy.

Oil and water are brought together in a T-section. The oil–water mixture then flows through a 3 m long flexible hose, which allows the rig inclination to be set at any angle between horizontal and vertical, before entering into the 0.1 m I.D., 14 m long (140 pipe diameters) stainless steel pipe allowing the flow pattern and wall wetting to develop and stabilize. The oil–water mixture then enters the so called "upstream" 2 m long mild steel test section, where most of the measurements are carried out. A 2 m long transparent pipe section follows, which is used to visualize the flow pattern. Subsequently, the oil–water mixture flows through a 180° bend, and enters into another 14 m long stainless steel pipe section, where the flow pattern and the wall wetting are allowed to reach equilibrium again. The flow then enters the so called "downstream" mild steel test section followed by another transparent pipe section. For inclined flow these two test sections are used for distinguishing water wetting in ascending and descending flows. In the case of horizontal flow they offer redundant information. When the oil–water mixture leaves the downstream test section, it flows to the oil–water separator. The oil and the water are then led back to their respectable storage tanks for further circulation.

The oil–water separator is a crucial element in the experimental setup and enables accurate separation and dosing of the individual liquids and prevents build-up of a stable oil–water suspension. Fig. 4 shows the internal structure of the oil–water separator with a capacity of 2000 l of liquids.

In order to enhance the separation efficiency, three main internal components are installed into the separator. A liquid distributor is set at the side close to the oil–water mixture inlet, which is used to distribute the oil–water mixture uniformly on the cross-section of the separator. A mesh-like droplet coalescer comes immediately after the liquid distributor; the coalescer is built from two materials with very different surface free energies, namely stainless steel and plastic, enabling more effective separation. Finally the liquids go through a series of plate separators, after which empty space allows for longer residence time in the separator, ensuring complete separation. The water is

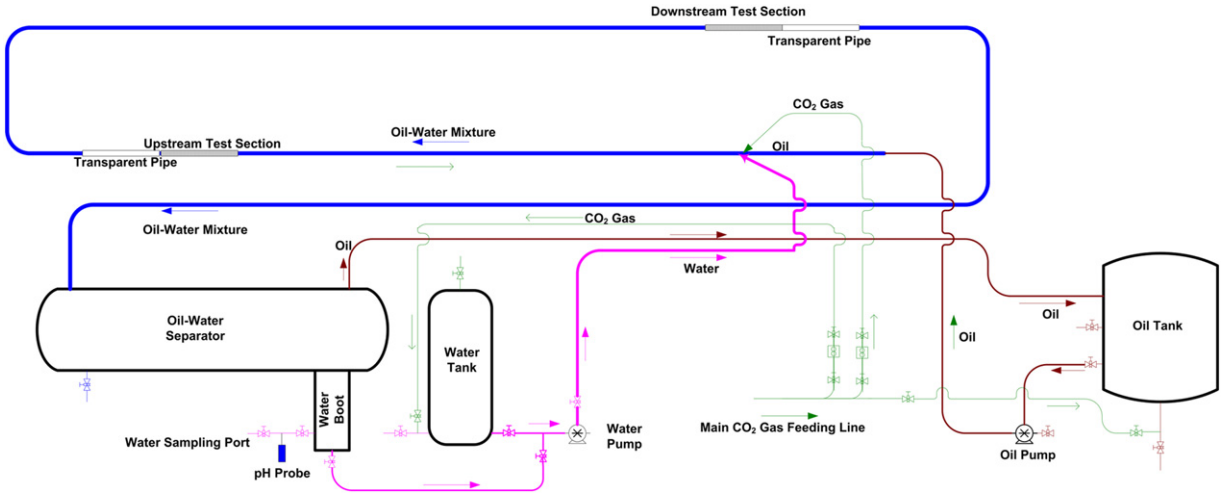

Fig. 3. Schematic of the inclinable flow loop used for the research. Oil and water are pumped separately and join in a 0.1 m pipe with a test section a and a transpartent section located at the end of a 14 m straight pipe section.

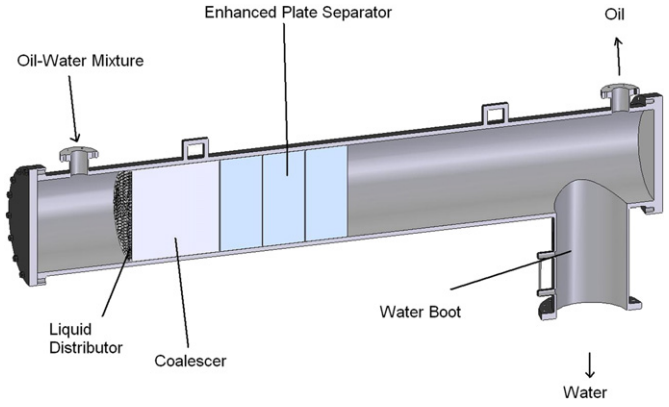

Fig. 4. Schematic cross-section of the oil–water separator including a liquid distributer, coalescer and plate separator.

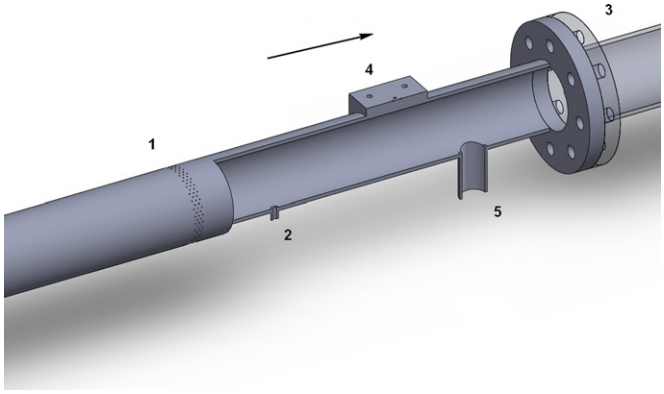

Fig. 5. Schematic of the test section showing the location of the different testing equipments with an arrow showing the direction of the flow. The equipment is located as follows: 1. Ports for conductivity pins, 2. Fluid sampling port, 3. Transparent pipe, 4. Saddle for High Frequency Impedance Probe and 5. Port for Electrical Resistance (ER) probe. The current study makes use of the conductivity pins, the wall sampling port and the transparent pipe.

accumulated in the water boot, before it flows back to the water tank and the oil is pushed up through the top back to the oil tank.

Since CO_2 corrosion rate measurements are carried out in this study, in order to minimize the effect of oxygen on the corrosion process, the system is deoxygenated using carbon dioxide (CO_2) before commencement of experiments. The deoxygenation process for this system takes approximately two and a half hours and results in an oxygen concentration below 25 ppb, measured with a visual colorimetric analysis (CHEMets). The pH in the system is maintained around pH at 4.8.

2.2. Instrumentation

Fig. 5 shows the schematic of the 2 m long mild steel test section used in the study. The test section corrodes during experiments, which leads to an increase of Fe^{2+} ion concentration in the water phase providing an indirect measurement of the corrosion rate. In addition the mild steel test section has conductivity pins, and a fluid sampling port. The mild steel test section is also designed to accommodate high frequency impedance probes, and an electrical resistance (ER) probe, but these were not a part of the current study.

In this study, four main techniques were used to determine phase wetting on the internal wall of pipe at different oil and water flow rates in the large diameter oil–water horizontal flow: flow pattern visualization, conductivity pins, fluid sampling and corrosion rate monitoring by iron counts (Fe^{2+} concentration).

Visual observations and recordings were conducted at the transparent test section just downstream of the main mild steel test section (Fig. 5). Artificial coloring of the water, by fluorescein sodium salt, was used to enhance the contrast between the phases under UV lighting. The macroscopic flow structure, i.e., the flow pattern, could be identified based on visual observations.

In this study special attention is paid to what happens at the internal pipe wall, i.e., to the interaction between fluids and the pipe surface, which was the main task of the experimental campaign. Therefore, an array of conductance pins was used to investigate the phase wetting along the circumference of the pipe internal wall. The probes are epoxy-coated stainless steel pins with 0.45 mm O.D. threaded through a 0.5 mm I.D. hole in the pipe wall (Fig. 6). Five staggered rows of 160 pins are flush-mounted on the entire circumference of the pipe wall (Fig. 5) for the "upstream" test section and 93 pins that are flush-mounted on the bottom half for the "downstream" test section. This particular arrangement with a large number of spatially distributed probes was used to avoid problems with the water phase "snaking" around individual probes, leading to false readings. Furthermore, this redundant configuration proved to be very

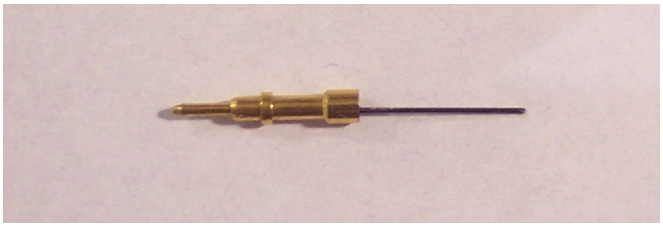

Fig. 6. One of the 160 conductivity pins, which are flush mounted on the internal wall of the mild steel test section.

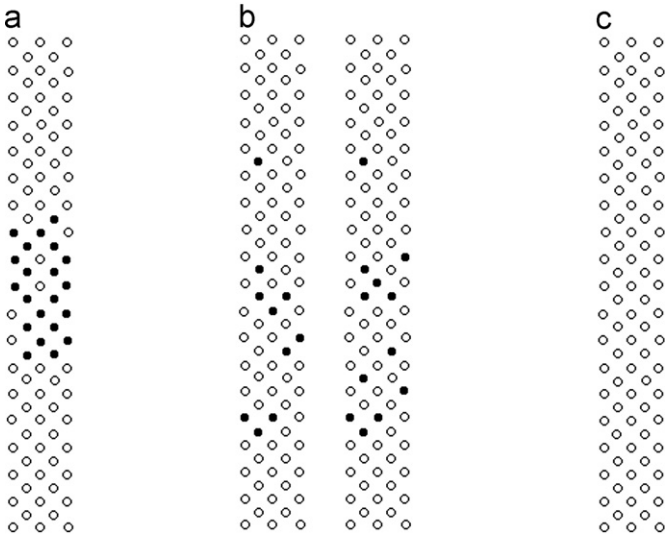

Fig. 7. Typical data for the conductivity pins distributed at the bottom half of the test section. It is displayed as a snapshot of simultaneous wetting of the pins, where an empty circle denotes oil wetting and a filled circle water wetting. The snapshots describe (a) stable water wetting, (b) intermittent wetting and (c) stable oil wetting. The bottom of the pipe corresponds to the vertical center of the pin snapshot.

useful for characterizing intermittent wetting and for eliminating experimental outliers.

The conductivity pins detect whether the fluid on top of them is conductive (water) or non-conductive (oil/air) using a voltage divider, of which the conducitivity pin is the bottom resistor and a 1 MΩ resistor as the top resistor. If a non-conductive fluid is in contact with the conductivity pin it forms a high resistance between the pin and the mild steel test section and the node voltage (between the 1 MΩ resistance and the pin) is the same as the excitation voltage. If a conductivity pin is covered with water the resistance between the pin and the mild steel test section is low and the node voltage is lower than the excitation voltage. This voltage is sent to a comparator to compare with a reference voltage, which can change depending on the salinity of the water. When the voltage is lower than the reference voltage the pin is determined to be wetted with water, otherwise it is wetted with oil. This information is collected from all of the pins simultaneously and each pin is displayed as either a filled circle if it is water wet or an empty circle if it is oil wet as seen in Fig. 7. The Figure shows the three different wetting regimes:

- *stable water wetting*: where at least a portion of the pipe wall is constantly wet with water (in the case of horizontal pipe flow it is the bottom), and corrosion is likely;
- *intermittent wetting*: where a portion of the pipe wall is periodically wet with water and oil in an alternating fashion, and corrosion is possible;
- *stable oil wetting*: where the whole pipe wall is constantly wet with oil, and corrosion is unlikely.

A fluid sampling method was used to measure the water and oil content very close to the surface of the pipe inner wall by extracting the fluid from the bottom of the pipe using a precisely controlled needle valve and a solenoid valve. The controlling instrumentation was carefully calibrated so that the proper extraction time and suction is applied to minimize erroneous readings. Slow sampling may lead to separation of the oil and water in the sampling tubing while aggressive suction draws liquid from the bulk of the flow, both distorting the picture about the oil/water ratio at vicinity of the wall. The amount of oil and water in the sampling tubes was estimated visually, with a measurement error as high as 100% at very high or low water contents ($<10\%$ water or $>90\%$ water) and as low as 10% at moderate water content (10–90% water).

Since a CO_2 saturated water/oil mixture is circulated through the flow loop, it is straightforward to conduct corrosion measurements in the mild steel test section. When water wets the inner wall of the carbon steel test section, corrosion is initiated according to

$$Fe_{(s)} + CO_{2(aq)} + H_2O_{(l)} \rightarrow Fe^{2+} + CO_3^{2-} + H_{2(g)} \quad (15)$$

This will manifest itself as a rise in dissolved ferrous ion (Fe^{2+}) concentration in the water phase, which can be detected by sampling the water and employing a spectrophotometer (so called "iron counts"). The iron count technique has a considerably longer response time (typically a few hours) for estimating phase wetting compared to the other methods discussed (typically a few seconds to a few minutes), and has an error of measurement of 20%.

It was anticipated that on using different techniques for the detection of phase wetting as described above, overlapping information will be obtained. This would increase the confidence in the overall conclusions and yield a stronger base for modeling of water wetting.

3. Results and discussion

The results of flow pattern visualization are discussed first, followed by the phase wetting results according to the conductivity pins. Those results are then compared and put in context with fluid sampling and iron corrosion rate (iron count) measurements.

3.1. Flow pattern map from visualization

Based on video images from a high speed image recorder, different flow patterns were identified at different flow conditions (Fig. 8). The superficial fluid velocity is calculated as a flow rate divided by the pipe cross section area, both for the oil, V_{so}, and water, V_{sw}. The total oil–water superficial velocity, V_{st} (Figs. 8(b) and 10(b)), is the combined velocity of oil and water ($V_{st}=V_{so}+V_{sw}$).

There are two dominant flow regimes depending on the oil superficial velocity, V_{so}: stratified and dispersed. It was found that when V_{so} is lower than 1.5 m/s, the flow is stratified but dispersed when V_{so} is 1.5 m/s or greater. Each flow regime is further divided into sub-categories:

- *stratified*:
  - stratified with water globules,
  - smooth stratified,
  - stratified with a mixing layer;
- *dispersed*:
  - semi-dispersed,
  - fully dispersed.

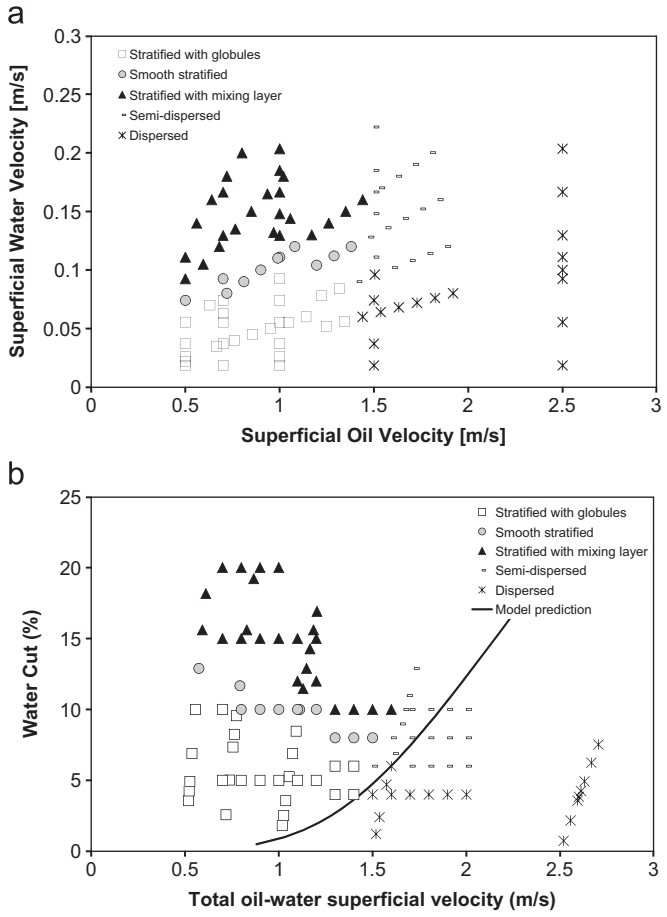

Fig. 8. Flow regime map of LVT200 oil–water flow in large diameter (0.1 m) horizontal pipe. The data is displayed in two ways (a) using superficial velocities and (b) using water cut and the total oil and water superficial velocity. The model prediction is included in the latter.

For the lowest water flow rates (superficial velocities V_{sw}), the water stream flows separated at the bottom of the horizontal line, but there is not enough water phase to produce a continuous water layer. Instead, the water is broken up into globules that flow at the pipe bottom (Fig. 9(a)). The size of the globules depends on the V_{so}, since increasing the superficial oil velocity increases the turbulence, which breaks the globules up into smaller globules which are eventually entrained and dispersed as water droplets in the bulk oil phase. As the superficial water velocity increases, the globules coalesce into a thin water layer at the bottom of the pipe at values of V_{sw} of around 0.07–0.1 m/s, depending on the V_{so}, and the flow pattern becomes smooth stratified. With increasing superficial water velocity, water droplets become entrained in the oil layer at the oil–water interface, and conversely, some oil droplets flow dispersed at the top of the water layer, at which point the flow regime becomes stratified with a mixing layer (Fig. 9(b)).

The dispersed flow was observed at $V_{so} \geq 1.5$ m/s (Fig. 8). At low V_{sw} (< 0.1 m/s), the flow was fully dispersed, and the water was evenly distributed across the cross section of the pipe. At V_{sw} greater than 0.1 m/s, the flow pattern is semi-dispersed, meaning that the entrained water droplets are more concentrated towards the bottom of the pipe, due to increased coalescence making larger water droplets so that they are pulled down more effectively by gravity. The model presented in Eqs. (6) and (7) for the transition between stratified and dispersed flow is included in Fig. 8(b) and shows a good match with the measured transition, especially at lower oil–water velocity, V_{st}.

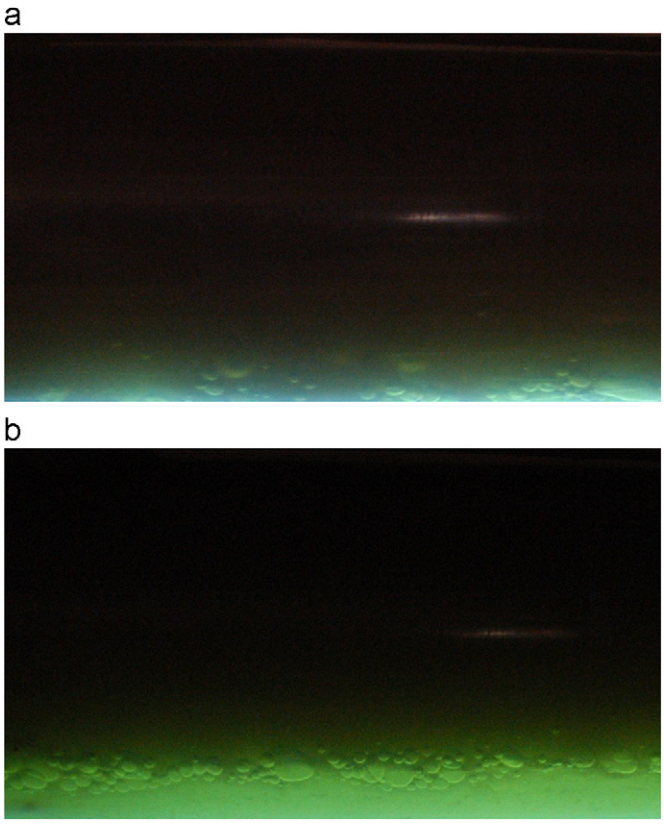

Fig. 9. Visualization of typical flow patterns at $V_{st}=0.5$ m/s, taken under UV light with fluorescein salt added to the water. (a) At $V_{sw}=0.025$ m/s (5% water cut) the water flows as globules at the bottom, (b) at $V_{sw}=0.1$ m/s (20% water cut) the flow is stratified with a mixing layer on top of the water layer.

Out of the five flow patterns reported in the current paper, three of them correspond to the flow patterns defined by Trallero (1995): *smooth stratified*, *stratified with mixing layer* and *dispersed*. The two flow patterns which deviate from the classification of Trallero are *stratified with globule*, which is not generally defined in the literature, but can be categorized as a variation of the *stratified* flow pattern for low water cuts, and *semi-dispersed*, which can fall under the definition of fully *dispersed* flow.

3.2. Phase wetting map from conductivity pins

The results obtained with the conductance probes identified three main phase wetting regimes, *stable water wetting*, *stable oil wetting* and *intermittent wetting*, described in Section 2.2. It should be stressed that in this terminology, it is sufficient that only a part of the pipe wall (often the bottom part) is wetted with water in order to use the term "water wetting", because this will likely lead to corrosion.

From Fig. 10 it appears that there is a threshold, i.e., for superficial oil velocity higher than 1.5 m/s, one gets full water entrainment, resulting in the steel surface being predominantly oil wet, with low likelihood of corrosion. At these high oil velocities the turbulent energy of the flow is sufficient to entrain the entire water phase. However, upon closer inspection one can see that at low oil velocities (< 1.5 m/s), oil wetting is also observed for very low water velocities ($V_{sw} < 0.03$ m/s). At these low water velocities, the water flows as globules at the bottom (Fig. 8), but is not able to wet the wall. As the V_{sw}, and thereby the water cut, is increased (keeping V_{so} in the range of 0.5–1.5 m/s) the water globules become bigger and heavier and start to wet bottom intermittently leading to the possiblity of corrosion.

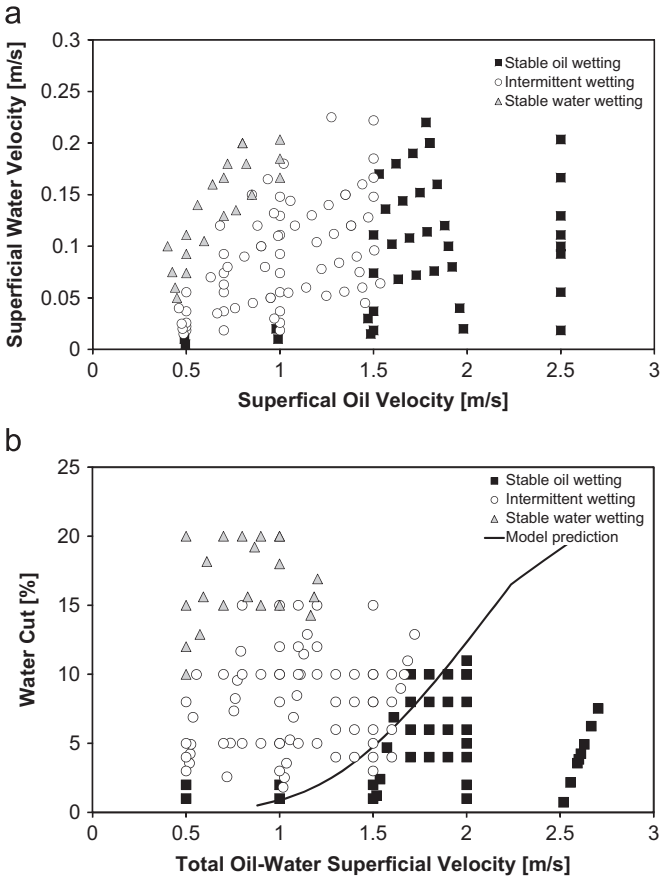

Fig. 10. Phase wetting map for LVT200 oil–water flow in large diameter (0.1 m) horizontal pipe. The data is displayed in two ways (a) using superficial velocities and (b) using water cut and the total oil–water superficial velocity. The model prediction is included in the latter.

As the water cut is increased further, stable water layer is formed at the bottom producing constant water wetting and increasing the likelihood of corrosion.

The wetting results obtained with the conductivity pins (Fig. 10) are consistent with the flow pattern observations (Fig. 8), where dispersed flow and stable oil wetting were observed for $V_{so} > 1.5$ m/s. Conversely, for $V_{so} < 1.5$ m/s, stratification of the flow is observed, where the water can either flow in a stable layer and wet the bottom of the pipe continuously, flow as large globules leading to intermittent wetting or be fully entrained by the oil phase resulting in stable oil wetting, all depending on the superficial water velocity, V_{sw}, i.e. the water cut.

Table 2 contains the result from both the flow pattern observation and the phase wetting measurements in a convenient format. It further emphasizes the strong correlation between the flow pattern and the phase wetting. Stable water wetting is only observed when the flow is stratified and stable oil wetting is only observed when the flow is dispersed. However, intermittent wetting can be observed for every flow pattern, except for fully dispersed flow.

3.3. Results of fluid sampling

Besides the results of the flow patterns and wetting regimes, Table 2 furthermore contains the results from fluid sampling from the bottom of the pipe. The fluid sampling is one more test method that was used to compare with the findings from both the visual observation and the conductance probe measurements.

It was shown that full water wetting is only observed when the water flows at the bottom of the pipe as a layer (rather than globules) and the fluid sample in this case shows 100% water. Even if only 1% of oil was found in the fluid sample (i.e. 99% water), this corresponded to intermittent wetting, apparently with the water in the form of rather large globules, which occasionally wet the pipe wall. When the water in the fluid sample showed between 99% and 40% water, intermittent wetting was observed while even in the stable oil wetting regime the water in the fluid sample was detected in the range of 1–20%.

As the water flow rate increases, the turbulence of the flow is insufficient to prevent coalescence of the water droplets, and the water droplets form larger and heavier droplets, which sink towards the bottom of the pipe. The fluid sampling picks up this tendency, since higher water ratio in the fluid sample is measured for higher water flow rate. If results from different oil velocities are compared (Table 2), it is found that 99% water is measured in the fluid sample for 3.6% water cut at 0.5 m/s compared to 75% water in the fluid sample for 3.6% water cut at 1.0 m/s.

Clearly, while the two are broadly consistent, the correlation between fluid sample composition and water wetting is not straightforward. One can speculate that fluid sampling, if used as a stand alone technique (without the aid of other techniques) would have offered ambiguous results (at best) and would be difficult to relate to pipe wall wetting.

3.4. Corrosion rate measurements

Since corrosion occurs as soon as water comes into contact with the steel surface, the transition between oil wetting and intermittent wetting is of great practical importance. No corrosion occurs when the pipe wall is steadily oil wet, while some corrosion is to be expected in the case of intermittent wetting, although the water is not constantly in contact with the pipe wall. Even more corrosion is to be expected in the stable water wetting regime.

As the test section in the flow loop is made out of mild steel while the rest of the flow loop is made out of non-corroding materials, corrosion under different wetting regimes could be assessed by monitoring the concentration of Fe^{2+} in the water phase—iron counts. The result from iron counts are shown in Table 3 with the iron count measurements taken after the flow regime has been kept constant for at least 30 min. They confirm that no corrosion was measurable when the stable oil wetting regime was maintained. In the intermittent water wetting regime some corrosion was observed as indicated by the clear increase in the iron counts.The corrosion rate was significantly higher (approximatey double) in the the stable water wetting regime.

Overall one can summarize that the corrosion process, as monitored by the change in the Fe^{2+} concentration in the water phase —iron counts, is an indispendable tool required to reinforce other types of the phase wetting measurements. However, one needs to remember that it is also an inconvenient technique particularly when used as a standalone phase wetting measurement indicator. The corrosion rate measurements are slow, and what is even more important—difficult to apply and interpret in a straightforward fashion. For example, when the corrosion rate is mass transfer/flow dependent (e.g. in the low pH range), this effect is difficult to distinguish from the water wetting effect. Another example the concentration of Fe^{2+} in the water phase will not increase nearly as much if a corrosion inhibitor is present, whether it is added to the system or it is naturally found in the oil being tested. In such cases, the result of corrosion inhibition can easily be confused with the change in water wetting—particualrly because both can happen at the same time and lead to a reduction in the corrosion rate. Even more difficulties are encountered in

Table 2
Comparison of results from conductivity pins (wetting maps), visual observation (flow regime maps) and fluid sampling for each superficial water and oil velocity.

V_{so} (m/s)	V_{sw} (m/s)	Water cut, ε (%)	Wetting regime	Flow regime	Fluid sampling (% water)	V_{so} (m/s)	V_{sw} (m/s)	Water cut, ε (%)	Wetting regime	Flow regime	Fluid sampling (% water)
0.5	0.019	3.6	Intermittent	Stratified w/globules	99	1.5	0.019	1.2	Oil	Dispersion	1
0.5	0.022	4.3	Intermittent	Stratified w/globules	99	1.5	0.037	2.4	Oil	Dispersion	1
0.5	0.026	4.9	Intermittent	Stratified w/globules	99	1.5	0.074	4.7	Oil	Dispersion	10
0.5	0.037	6.9	Intermittent	Stratified w/globules	99	1.5	0.11	6.9	Oil	Semi-dispersed	20
0.5	0.056	10.0	Intermittent	Stratified w/globules	99	1.5	0.15	9.0	Intermittent	Semi-dispersed	40
0.5	0.074	12.9	Water	Smooth stratified	100	1.5	0.17	10.0	Intermittent	Semi-dispersed	40
0.5	0.093	15.6	Water	Stratified w/mixed layer	100	1.5	0.19	11.0	Intermittent	Semi-dispersed	60
0.5	0.11	18.2	Water	Stratified w/mixed layer	100	1.5	0.22	12.9	Intermittent	Semi-dispersed	60
0.7	0.019	2.6	Intermittent	Stratified w/globules	99	2.5	0.019	0.73	Oil	Dispersion	5
0.7	0.037	5.0	Intermittent	Stratified w/globules	99	2.5	0.056	2.2	Oil	Dispersion	5
0.7	0.056	7.3	Intermittent	Stratified w/globules	99	2.5	0.093	3.6	Oil	Dispersion	4
0.7	0.063	8.2	Intermittent	Stratified w/globules	99	2.5	0.10	3.8	Oil	Dispersion	2
0.7	0.074	9.6	Intermittent	Stratified w/globules	99	2.5	0.11	4.3	Oil	Dispersion	2
0.7	0.093	11.7	Intermittent	Smooth stratified	100	2.5	0.13	4.9	Oil	Dispersion	2
0.7	0.13	15.6	Water	Stratified w/mixed layer	100	2.5	0.17	6.2	Oil	Dispersion	2
0.7	0.17	19.2	Water	Stratified w/mixed layer	100	2.5	0.20	7.5	Oil	Dispersion	2
1.0	0.019	1.8	Intermittent	Stratified w/globules	5						
1.0	0.026	2.5	Intermittent	Stratified w/globules	50						
1.0	0.037	3.6	Intermittent	Stratified w/globules	75						
1.0	0.056	5.3	Intermittent	Stratified w/globules	90						
1.0	0.074	6.9	Intermittent	Stratified w/globules	95						
1.0	0.093	8.5	Intermittent	Stratified w/globules	99						
1.0	0.11	10.0	Intermittent	Smooth stratified	99						
1.0	0.13	11.5	Intermittent	Stratified w/mixed layer	99						
1.0	0.15	12.9	Intermittent	Stratified w/mixed layer	99						
1.0	0.17	14.3	Water	Stratified w/mixed layer	100						
1.0	0.19	15.6	Water	Stratified w/mixed layer	100						
1.0	0.20	16.9	Water	Stratified w/mixed layer	100						

Table 3
Change in Fe^{2+} concentration measured for different wetting regimes after 30 min exposure.

Phase wetting	Fe^{2+} change (ppm)	Oil–water mixture velocity (m/s)	Water cut (%)
Water wetting	1.32	0.6	16
Intermittent wetting	0.57	0.8	14
Oil wetting	0	1.6	7

those conditions where an iron cabonate corrosion product layer forms (at higher pH and higher temperature) when the corrosion rate, concentration of Fe^{2+} in the bulk water phase and the wettability of an iron carbonate covered steel surface change in a complicated way and make it difficult to reach a valid conclusion.

4. Modeling

The experimental results shown above already suggests that even in this "simplest of cases" one cannot deduce a simple criterion for water wetting and that the "rule-of-thumb" approach, used previously by the industry, is bound to fail. For example the common criterion, where oil wetting is expected to occur at flow rates above 1 m/s and water cuts below 30% is clearly not valid in this case. Both the visual observations and the phase wetting measurements suggest that there may be some sort of threshold, i.e. at 1.5 m/s, however it is lower for low water cuts. Even more importantly, all the values reported above are valid only for the given type of oil (with its given properties) and this diameter and inclination of the line, and that very different results would be obtained if any of these changed (as suggested in the parametric analysis shown in Fig. 2, and confirmed with further experimentation).

On the other hand, the mechanistic model described above performs reasonably well. For example Fig. 10(b) includes a model prediction, based on the water entrainment model (Eqs. (6) and (7)). The model accurately calculates the transition between stable oil wetting and water wetting, which happens when the wetting regime changes from oil wetting to intermittent wetting. The results displayed in Table 3 verify that this transition (oil wetting to intermittent wetting) is also the transistion between corrosive and non-corrosive conditions. The model (Fig. 10(b) sucessfully captures the change in wetting found at very low water cuts ($<2\%$ water cut), something that is not possible to conclude by looking at the map of flow patterns alone (Fig. 8).

It is important to stress, that it is not claimed here, that the model in its present from is universally applicable to all other situations and fluids, including flow of heavier crude oils and other oil–water chemistries containing surface active compounds. However, the present model is a major step forward when compared to the various rules of thumb and empirical models previously used. Also, as it is mechanistic in nature, the model should relatively be easy to accommodate improvements which will likely be required to account for new phenomena observed under different conditions.

5. Conclusions

A water entrainment model, based on the transition between stratified and dispersed flow, has been suggested for oil–water two phase flow. This model can be used successfully to predict the transition between stratified and dispersed flow, and between oil

and water wetting. The assumption that oil wetting occurs when the water phase is fully dispersed in the oil is substantiated, as well as the assumption that stable oil wetting will lead to zero corrosion. Since the model is based on the physical behaviors of the flow, it can be used to gain understanding of what will happen when one, or more, of the parameters are changed. Lower entrainment velocities would be obtained with smaller diameter pipes, higher inclination (upwards or downwards), higher oil viscosity and density and lower interfacial tension.

The conductivity pins were proved to be a reliable and effective method to assess the surface wetting, as the results were backed up by other measurement techniques (fluid sampling, visual observation and Fe^{2+} concentration). Using the conductivity pins, three different wetting regimes were identified: water wetting, intermittent wetting and oil wetting. Corrosion was not detected under stable oil wetting conditions and was considerably lower under intermittent wetting conditions than stable water wetting.

Acknowledgment

The authors would like to acknowledge Saudi Aramco for funding this research program and Mr. Albert Schubert, the Institute's laboratory director, for his technical assistance and design of the instrumentation.

References

Adams, C.D., Garber, J.D., Walters, F.H., Singh, C., 1993. Verification of computer modeled tubing life predictions by field data. In: Proceedings of Corrosion/93, Paper no. 82. NACE, Houston, TX.

Angeli, P., Hewitt, G.F., 2000. Flow structure in horizontal oil–water flow. Int. J. Multiphase Flow 26 (7), 1117–1140.

Bannwart, A.C., Rodriguez, O.M.H., de Carvalho, C.H.M., Wang, I.S., Vara, R.M.O., 2004. Flow patterns in heavy crude oil–water flow. J. Energy Resour. Technol.—Trans. ASME 126 (3), 184–189.

Barnea, D., 1986. Transition from annular-flow and from dispersed bubble flow—unified models for the whole range of pipe inclinations. Int. J. Multiphase Flow 12 (5), 733–744.

Barnea, D., Shoham, O., Taitel, Y., 1982. Flow pattern transition for vertical downward 2 phase flow. Chem. Eng. Sci. 37 (5), 741–744.

Bond, W.N., Newton, D.A., 1928. Bubbles, drops, and Stokes' Law. London Edinborough Dublin Philos. Mag. 5, 794–800. (Paper 2).

Brauner, N., 2001. The prediction of dispersed flows boundaries in liquid–liquid and gas–liquid systems. Int. J. Multiphase Flow 27 (5), 885–910.

Brauner, N., Moalem Maron, D., 1992. Flow pattern transitions in two-phase liquid–liquid flow in horizontal tubes. Int. J. Multiphase Flow 18 (1), 123–140.

Brauner, N., Ullmann, A., 2002. Modeling of phase inversion phenomenon in two-phase pipe flows. Int. J. Multiphase Flow 28, 1177–1204.

Brodkey, R.S., 1995. The Phenomena of Fluid Motions. Dover Publications, New York.

Charles, M.E., Govier, G.W., Hodgson, G.W., 1961. The horizontal pipeline flow of equal density oil–water mixtures. Can. J. Chem. Eng., 27–36.

de Waard, C., Lotz, U., 1993. Prediction of CO_2 corrosion of carbon steel. In: Proceedings of Corrosion/93, Paper no. 69. NACE, Houston, TX.

de Waard, C., Smith, L., Craig, B.D., 2001. The influence of crude oil on well tubing corrosion rates. In: Proceedings of EUROCORR 2001, October 30, Riva del Garda, Italy.

Efird, K.D., Jasinski, R.J., 1989. Effect of the crude-oil on corrosion of steel in crude-oil brine production. Corrosion 45 (2), 165–171.

Hernandez, S., Bruzual, J., Lopez-Linares, F., Luzon, J.G., 2003. Isolation of potential corrosion inhibiting compounds in crude oil. In: Proceedings of Corrosion/03, Paper no. 03330. NACE, Houston, TX.

Hernandez, S., Duplat, S., Vera, J., Baron, E., 2002. A statistical approach for analyzing the inhibiting effect of different types of crude oil in CO_2 corrosion of carbon steel. In: Proceedings of Corrosion/02, Paper no. 02293. NACE, Houston, TX.

Hinze, J.O., 1955. Fundamentals of the hydrodynamic mechanism of splitting in dispersion processes. AIChE J. 1 (3), 289–295.

Institute for Corrosion and Multiphase Technology, 2007. MULTICORP, V4.2. Ohio University.

Jepson, W.P., Taylor, R.E., 1993. Slug flow and its transitions in large-diameter horizontal pipes. Int. J. Multiphase Flow 19 (3), 411–420.

Knudsen, J.G., Katz, D.L.V., 1954. Fluid Dynamics and Heat Transfer. University of Michigan.

Kumara, W.A.S., Halvorsen, B.M., Melaaen, M.C., 2009. Pressure drop, flow pattern and local water volume fraction measurements of oil–water flow in pipes. Meas. Sci. Technol. 20, 11.

Mandal, T.K., Chakrabarti, D.P., Das, G., 2007. Oil water flow through different diameter pipes—similarities and differences. Trans IChemE Part A Chem. Eng. Res. Des. 85 (A8), 1123–1128.

Mendez, C., Duplat, S., Hernandez, S., Vera, J., 2001. On the mechanism of corrosion inhibition by crude oils. In: Proceedings of Corrosion/01, Paper no. 01044. NACE, Houston, TX.

Nadler, M., Mewes, D., 1997. Flow induced emulsification in the flow of two immiscible liquids in horizontal pipes. Int. J. Multiphase Flow 23 (1), 55–68.

Nesic, S., Postlethwaite, J., Olsen, S., 1996. An Electrochemical model for prediction of corrosion of mild steel in aqueous carbon dioxide solutions. Corrosion (Houston) 52 (4), 280–294.

Nordsveen, M., Nesic, S., Nyborg, R., Stangeland, A., 2003. A mechanistic model for carbon dioxide corrosion of mild steel in the presence of protective iron carbonate films—part 1: theory and verification. Corrosion 59 (5), 443–456.

Pots, B.F.M., John, R.C., Rippon, I.J., Simon Thomas, M.J.J., Kapusta, S.D., Girgis, M.M., Whitham, T., 2002. Improvements on deWaard–Williams corrosion prediction and applications to corrosion management. In: Proceedings of Corrosion/02, Paper no. 02235. NACE, Houston, TX.

Rodriguez, O.M.H., Oliemans, R.V.A., 2006. Experimental study on oil–water flow in horizontal and slightly inclined pipes. Int. J. Multiphase Flow 32 (3), 323–343.

Simmons, M.J.H., Azzopardi, B.J., 2001. Drop size distributions in dispersed liquid–liquid pipe flow. Int. J. Multiphase Flow 27, 843–859.

Simon Thomas, M.J.J., de Waard, C., Smith, L.M., 1987. Controlling factors in the rate of CO_2 corrosion. In: Proceedings of Corrosion'87, 26–28 October, Brighton, UK, pp. 147–159.

Trallero, J.L., 1995. Oil–water Flow Patterns in Horizontal Pipes. Ph.D. Dissertation.

Trallero, J.L., Sarica, C., Brill, J.P., 1996. A study of oil–water flow patterns in horizontal pipes. In: Proceedings of the SPE Annual Technical Conference and Exhibition, Paper no. 36609, 6–9 October 1996, Denver, Colorado, USA, pp. 363–375.

Utvik, O.H., Rinde, T., Valle, A., 2001. An experimental comparison between a recombined hydrocarbon–water fluid and a model fluid system in three-phase pipe flow. J. Energy Resour. Technol.—Trans. Asme 123 (4), 253–259.

Wegmann, A., von Rohr, P.R., 2006. Brief communication: two phase liquid–liquid flows in pipes of small diameters. Int. J. Multiphase Flow 32, 1017–1028.

Wicks, M., Fraser, J.P., 1975. Entrainment of water by flowing oil. Mater. Perform. 14 (5), 9–12.

Wu, Y., 1995. Entrainment method enhanced to account for oil's water content. Oil Gas J. 93 (35), 83–86.

Xu, X.-, 2007. Study on oil–water two-phase flow in horizontal pipelines. J. Pet. Sci. Eng. 59, 43–58.